UNIVERSITY OF WEST BOHEMIA

Applied and Computational Mechanics 1 (2007) 255 - 264

Applied and Computational Mechanics

Flow characteristics of curved ducts

P. Rudolf [a]*, M. Desová [a]

[a] *Faculty of Mechanical Engineering, Brno University of Technology,Technická 2,616 69 Brno, Czech Republic*

Received 10 September 2007; received in revised form 1 October 2007

Abstract

Curved channels are very often present in real hydraulic systems, e.g. curved diffusers of hydraulic turbines, S-shaped bulb turbines, fittings, etc. Curvature brings change of velocity profile, generation of vortices and production of hydraulic losses. Flow simulation using CFD techniques were performed to understand these phenomena. Cases ranging from single elbow to coupled elbows in shapes of U, S and spatial right angle position with circular cross-section were modeled for Re = 60000. Spatial development of the flow was studied and consequently it was deduced that minor losses are connected with the transformation of pressure energy into kinetic energy and vice versa. This transformation is a dissipative process and is reflected in the amount of the energy irreversibly lost. Least loss coefficient is connected with flow in U-shape elbows, biggest one with flow in S-shape elbows. Finally, the extent of the flow domain influenced by presence of curvature was examined. This is important for proper placement of mano- and flowmeters during experimental tests. Simulations were verified with experimental results presented in literature.

Keywords: curvature, hydraulic loss, vortex , Coriolis number, energy transformation

1. Introduction and objectives

Flows with curvature are very common in engineering applications. They can be found in most of the e.g. fittings, HVAC appliances, turbine and blade passages, etc.

Our objective is the investigation of curved flow as a preliminary study for design of curved diffusers. Curved diffuser called elbow draft tube is the exit part of hydraulic turbine and exhibits very complex flow. It is a combination of flow with curvature, adverse pressure gradient diffuser flow and swirling flow. We decided to divide this complexity into these basic flow types and study them separately before going to full simulation.

A lot of experimental and computational investigations have been carried out in past on curved ducts with rectangular cross-sections, e.g. [4], [7], [8], [9], much less effort was devoted to circular cross-sections, which are connected with problems particularly in experimental work, see [2], [10], [11]. But still there are discrepancies as for the integral flow characteristics and spatial evolution of the flow, especially if confronted with classical references [5], [6]. Aim of this paper is to find connections between integral characteristics (e.g. loss coefficient) and details of the flow field.

2. Geometry and flow parameters

All geometrical configurations of curved ducts have similar dimensions: same diameter d, same curvature radius $R = 2d$, same inflow and outflow length of the straight pipes, see fig.

*Corresponding author. Tel.: +420 541 142 336, e-mail: rudolf@fme.vutbr.cz.

Reynolds number based on the bulk velocity and pipe diameter is:

$$\mathrm{Re} = \frac{U_{m,ax}.d}{\nu} = 60000 \tag{1}$$

Curvature is characterized by Dean number:

$$De = \mathrm{Re}\sqrt{\frac{d}{2.R}} = 30000 \tag{2}$$

All parameters are in correspondence with experiment [10]. Cross-sections in bends are labeled according to fig.2. Labelling is similar for spatial 90-degrees bend, and angle ϕ without any subscript is used for single bend.

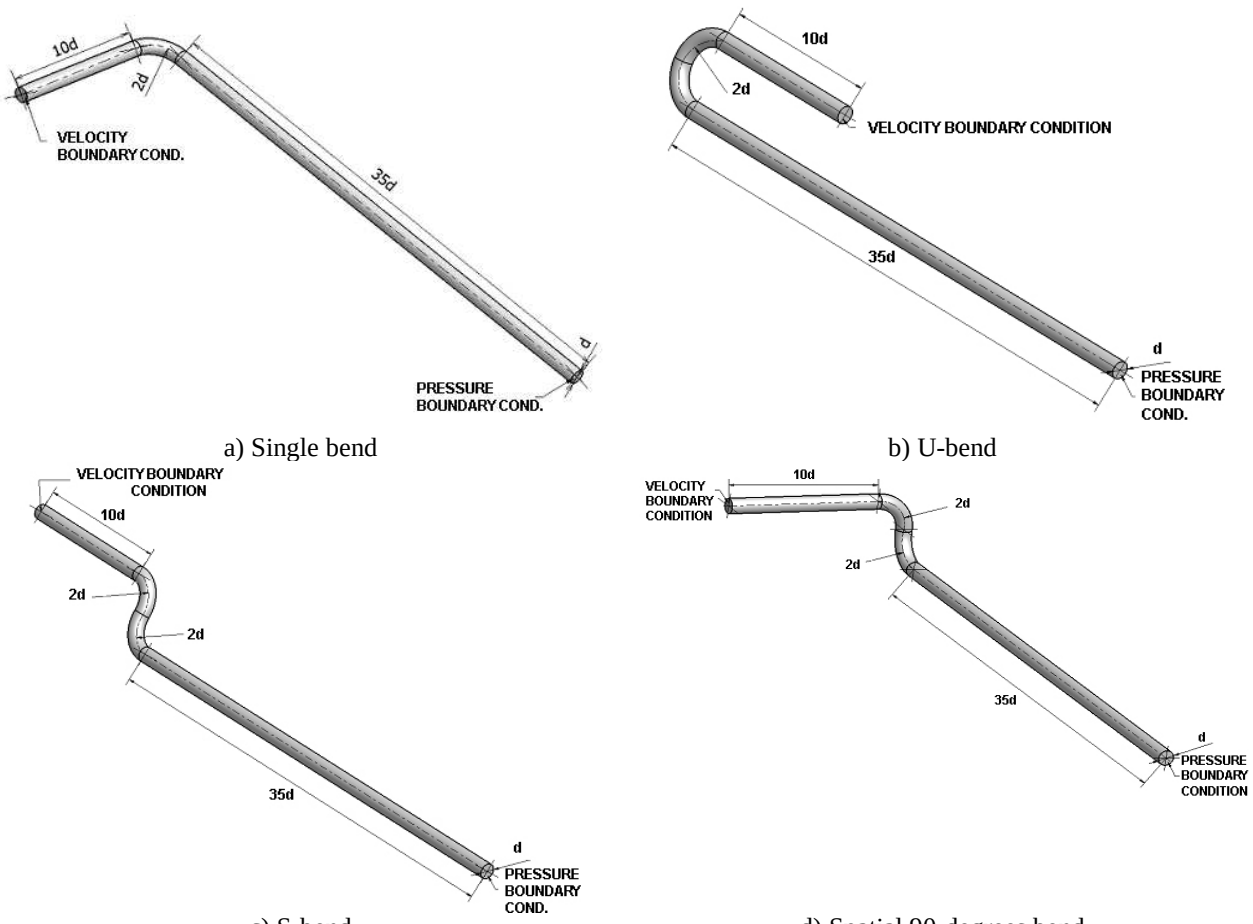

Fig.1. Geometrical configurations.

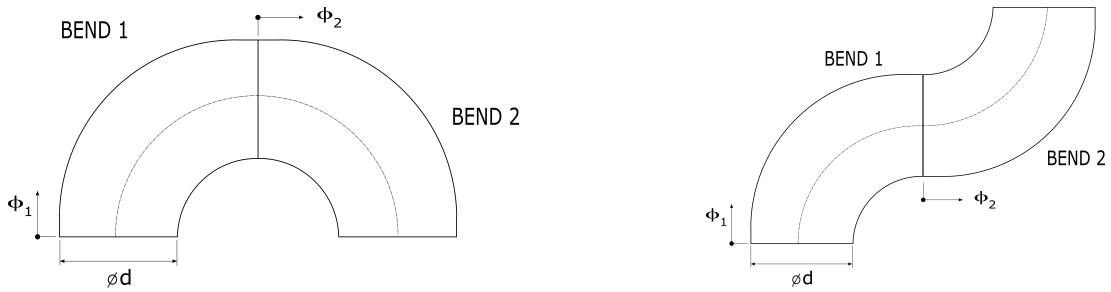

Fig.2. Labelling of the cross-sections.

3. Computational model

3.1. Governing equations and turbulence model

Finite volume solver Fluent 6.2 code [3] was used for computational simulation. Flow of incompressible fluid is governed by Reynolds averaged Navier-Stokes equations (RANS) and continuity equation.

Two-layer approach is employed for turbulence modeling. The core region is modeled using high-Reynolds realizable k-ε turbulence model. This model is a modification of standard k-ε turbulence model. The main difference lies in Prandtl-Kolmogorov relation, where C_μ is no longer a constant and becomes a function of turbulent kinetic energy, strain-rate tensor and rotation tensor (see eq.(6)) and a new transport equation for dissipation rate ε is formulated (see eq. (3))

$$\frac{\partial}{\partial t}(\rho\varepsilon)+\frac{\partial}{\partial x_j}(\rho\varepsilon U_j)=\frac{\partial}{\partial x_j}\left[\left(\mu+\frac{\mu_t}{\sigma_\varepsilon}\right)\frac{\partial\varepsilon}{\partial x_j}\right]+\rho C_1 S\varepsilon-\rho C_2\frac{\varepsilon^2}{k+\sqrt{\nu\varepsilon}}\ , \tag{3}$$

$$C_1=\max\left[0.43,\frac{\eta}{\eta+5}\right],\ \eta=S\frac{k}{\varepsilon},\ S=\sqrt{2S_{ij}S_{ij}}\ , \tag{4}$$

$$\tau_{t,ij}=\frac{\partial}{\partial x_j}\left(\mu_t\frac{\partial U_j}{\partial x_j}\right),\ \mu_t=\rho C_\mu\frac{k^2}{\varepsilon}\ , \tag{5}$$

$$C_\mu=\frac{1}{A_0+A_S\dfrac{kU^*}{\varepsilon}},\ U^*=\sqrt{S_{ij}S_{ij}-\Omega_{ij}\Omega_{ij}},\ A_0=4.04,\ A_S=\sqrt{6}\cos\phi\ , \tag{6}$$

$$\phi=\frac{1}{3}\cos^{-1}\left(\sqrt{6}W\right),\ W=\frac{S_{ij}S_{jk}S_{ki}}{\tilde{S}^3},\ \tilde{S}_{ij}=\sqrt{S_{ij}S_{ij}}\ , \tag{7}$$

$$S_{ij}=\frac{1}{2}\left(\frac{\partial U_i}{\partial x_j}+\frac{\partial U_j}{\partial x_i}\right),\ \Omega_{ij}=\frac{1}{2}\left(\frac{\partial U_i}{\partial x_j}-\frac{\partial U_j}{\partial x_i}\right), \tag{8}$$

$$C_{1\varepsilon}=1.44\ ,\ C_2=1.9\ ,\ \sigma_k=1\ ,\ \sigma_\varepsilon=1.2\ . \tag{9}$$

Improvement of this model over its standard form is in prediction of boundary layer flows under strong pressure gradients, separation, strong streamline curvature, recirculation, flow with presence of vortices.

Region in vicinity of walls is solved using one-equation Wolfshtein model. Turbulent viscosity is defined according to relation:

$$\mu_t=\rho C_\mu l_\mu\sqrt{k}\ , \tag{10}$$

k is obtained from differential transport equation and length scale from relation:

$$l_\mu=yK_1\left(1-\exp(-\mathrm{Re}_y/A_\mu)\right). \tag{11}$$

Dissipation term in transport equation for turbulent kinetic energy is obtained from:

$$\varepsilon=\frac{k^{3/2}}{l_\varepsilon}\ ,\ l_\varepsilon=yK_1\left(1-\exp(-\mathrm{Re}_y/A_\varepsilon)\right). \tag{12}$$

Reynolds number Re_y is defined using wall normal distance y:

$$\mathrm{Re}_y=\frac{y\sqrt{k}}{\nu}\ . \tag{13}$$

Value of Re_y is used as the switching criterion between high- and low-Reynolds regions, i.e. to realize switching between two-equation realizable k-ε model and one-equation Wolfshtein model.

3.2. Numerical algorithm, boundary conditions, computational grid

Computational domain is discretized using finite volumes. QUICK interpolation scheme is employed for convective term in momentum equation, central differencing for diffusive terms. Pressure-velocity coupling is via SIMPLE algorithm.

Inlet velocity boundary condition is obtained by simulation of the flow with same Reynolds number in sufficiently long straight pipe. Turbulence intensity for this simulation is estimated to be 2%, because this quantity is not presented in [10]. Constant static pressure is prescribed at the outlet. Rest of the domain is made of no-slip walls.

Hexahedral computational grid was created with about 800.000 volumes. Further adaption, enforced by near wall modeling, led to final number of 1.500.000 computational volumes. All cells in wall vicinity lie in viscous sublayer ($y^+ < 5$).

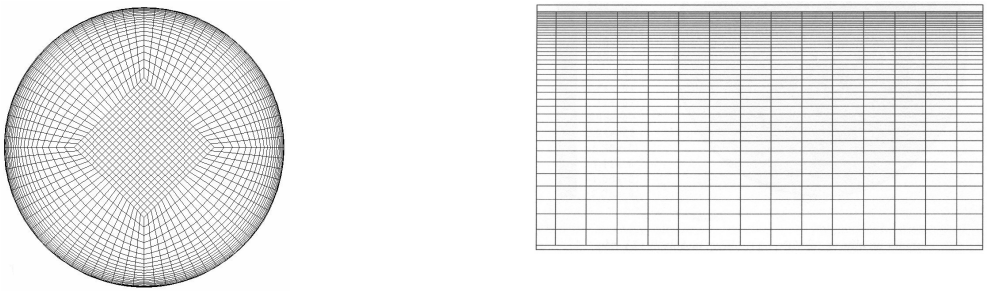

Fig.3. Cross-section of the computational domain (left) and zoom of the near wall region (right).

4. Integral flow characteristics

Integral flow characteristics are obtained using mean integral value theorem on selected cross-sections. Basic integral quantities are mean pressure and mean velocity, [1]. Coriolis number and loss coefficients are derived quantities

$$p_m = \frac{1}{Q}\int_0^Q p dQ \ , \ U_m = \frac{1}{S}\int_0^S U dS \ . \tag{14}$$

Correction for real specific kinetic energy of velocity profile is realized by Coriolis number, which is a ratio of kinetic energies of the real and ideal ("piston") velocity profiles:

$$\alpha = \frac{\int_0^S U_{m,ax} U_m^2 dS}{U_{m,ax}^3 . S} \ . \tag{15}$$

Specific energy of hydraulic losses is composed of two parts: friction losses and minor losses

$$E_L = E_{L,f} + E_{L,m} \ . \tag{16}$$

Friction losses represent internal friction in fluids flowing through straight pipes. Minor losses are associated with energy dissipation, usually caused by vortices and flow recirculation, in elements inserted in between the straight sections.

Friction loss must be computed first, if minor loss should be extracted from eq.(16)

$$f = \frac{E_{L,f}}{\frac{L}{d}\frac{U_{m,ax}^2}{2}} \quad . \tag{17}$$

Developed turbulent flow in a straight pipe was numerically simulated in present case to obtain friction factor f and verified with empirical relationships. Good agreement confirms that computational grid is sufficiently fine.

	relationship	friction factor *f*
Konakov	$f = \frac{1}{(1{,}8 \cdot \log \mathrm{Re} - 1{,}5)^2}$	0,019834
Nikuradse	$f = 0{,}0032 + \frac{0{,}221}{\mathrm{Re}^{0{,}237}}$	0,019492
Computational simulation	-	0,019595

Tab.1. Friction factor.

Total loss coefficient is computed from following expression:

$$K = \frac{\frac{p_{m,1}}{\rho} - \frac{p_{m,2}}{\rho} + \alpha_1 \frac{U_{m,1}^2}{2} - \alpha_2 \frac{U_{m,2}^2}{2}}{\frac{U_{m,1}^2}{2}} \quad . \tag{18}$$

And finally minor loss is defined by:

$$K_m = K - f \quad . \tag{19}$$

5. Single bend

Flow in curved duct invokes centrifugal force that is balanced by radial pressure gradient. Fluid particles along axis, with higher momentum are displaced to the outer (concave) curvature radius. On the other hand, low momentum particles in boundary layers on upper and lower walls are displaced in opposite direction to fulfill continuity equation. This process is origin of so called channel vortices, which form a characteristic vortex pair, see fig.4.

Comparison with experimental data [10] can be performed. Maximum velocity is near inner (convex) radius in both simulation and experiment slightly behind elbow inlet. This peak starts to shift towards concave side at about $\phi = 30°$ in experiment, whereas remains at the same position in simulation. Velocity maximum moves to concave side at $\phi = 60°$ in simulation. Ratio of maximum and mean velocity at bend exit is higher in simulation than in experiment. Flow field is more uniform at position 10*d* in experimental data. Overall it may be concluded that flow recovers faster in reality than in computational simulation. The possible reasons are wrong estimation of inlet turbulence intensity (not supplied in [8]), infidelity of physical model and numerical inaccuracy.

Details of the flow field are closely related to integral characteristics. Specific kinetic energy profile features two maxima, one behind bend inlet and the other behind bend exit. Decrease of kinetic energy after the second peak is even below the inlet value. Equalization to original value is reached at position 35.*d*. Specific pressure energy behaves inversely. Figure reveals transformation of pressure energy to kinetic energy and again to pressure energy. This

irreversible process is connected with energy dissipation and is the primary cause of the minor loss in curved ducts. Situation is also well depicted in Coriolis number profile, see fig.9.

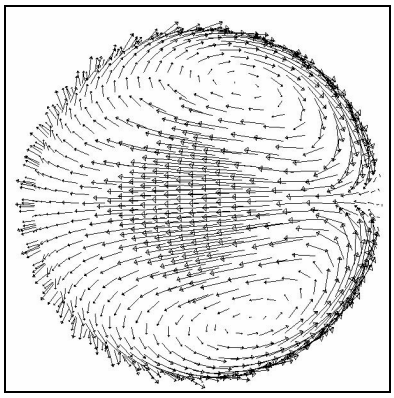

Fig.4. Velocity vectors for $\phi = 90°$ (view downstream, vector scale = 0.5).

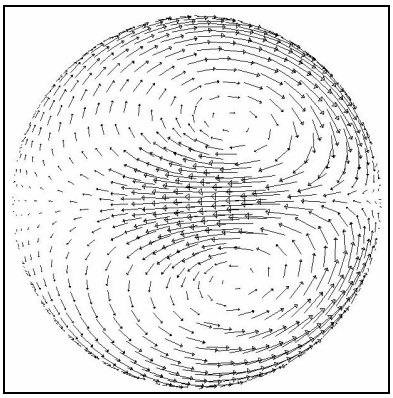

Fig.5. Velocity vectors at 5d behind bend (view downstream, vector scale = 1).

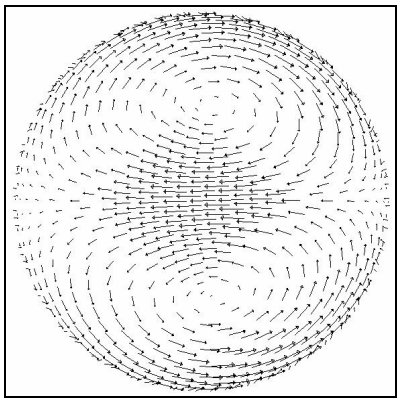

Fig.6. Velocity vectors at 25d behind bend (view downstream, vector scale = 4).

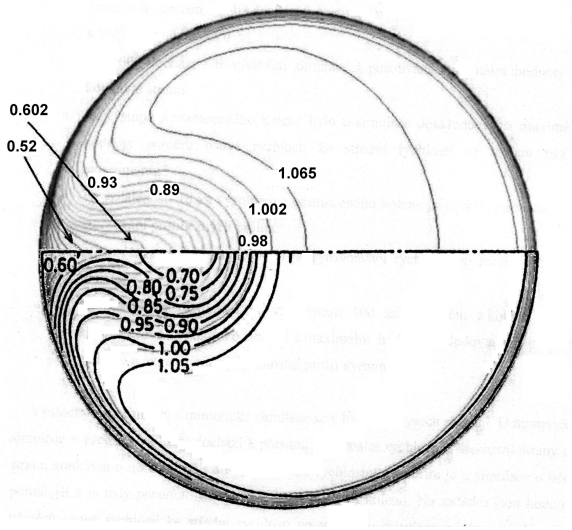

Fig.7. Velocity vectors for $\phi = 90°$ (up - computation, down - experiment [8], view upstream).

6. Compositions of bends

6.1 U-bend

Radial pressure gradient arises at the first bend inlet and consequently vortex pair is created. Vortex pair shifts to the inner curvature radius after passing through half of the first bend and is growing at the same time. This causes pushing of the low momentum fluid from the convex towards concave side accompanied by axial velocity drop on the concave side. Because this fluid has low momentum to overcome pressure gradient, it turns backwards and new pair of vortices originates, see fig.11. Continuity equation must be fulfilled and fluid near walls starts to move from the inner to outer radius. This process suppresses original vortex pair. New vortex pair causes faster recovery of the velocity field. Kinetic energy profile is characterized by one maximum and one minimum. Therefore the minor hydraulic loss is also low.

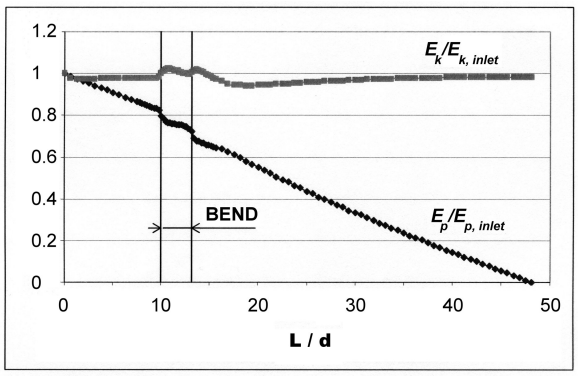

a) Single bend

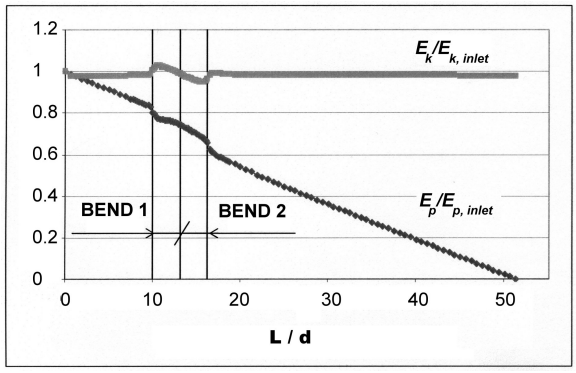

b) U-bend

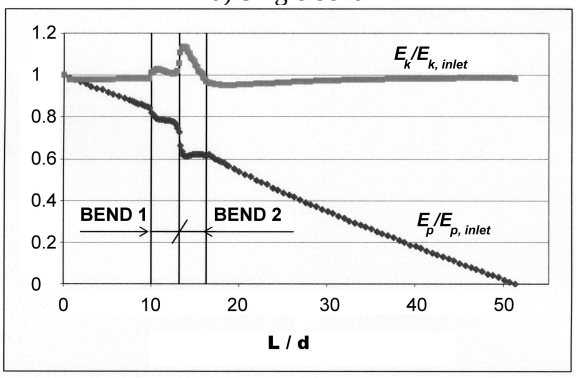

c) S-bend

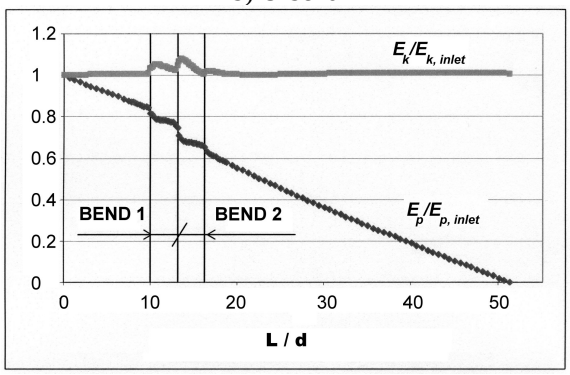

d) Spatial 90-degrees bend

Fig.8. Specific pressure and kinetic energies.

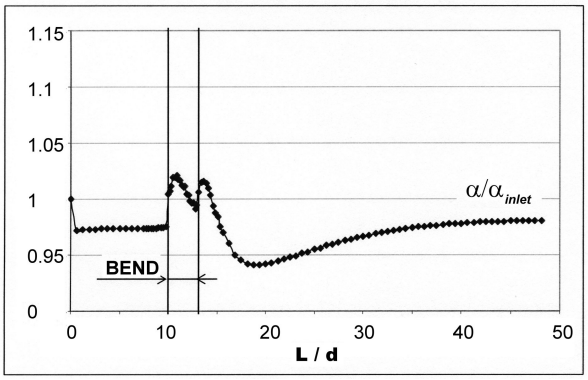

a) Single bend

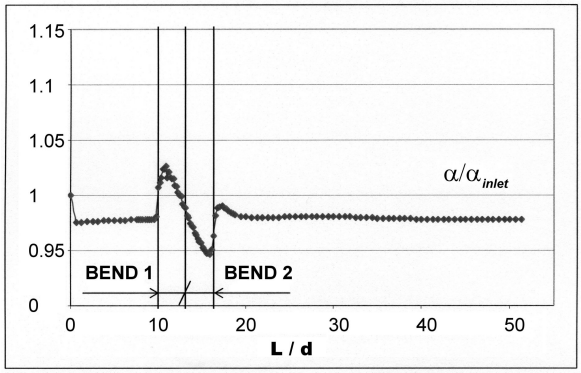

b) U-bend

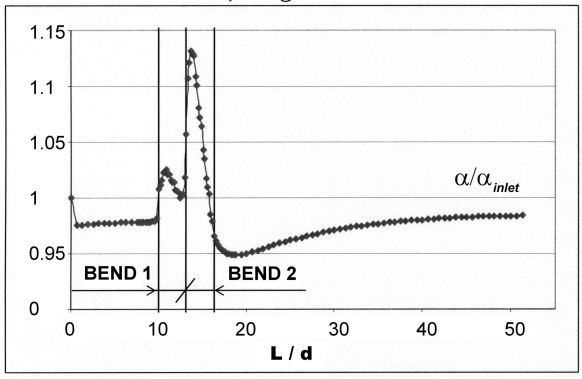

c) S-bend

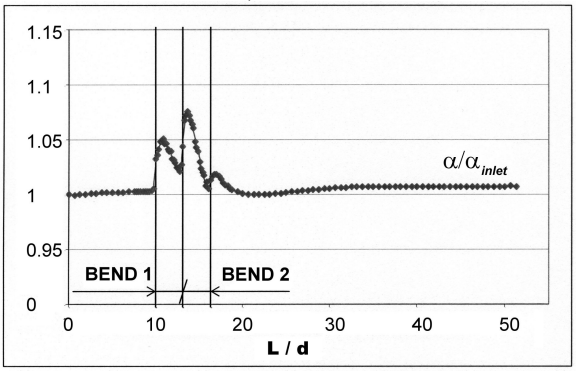

d) Spatial 90-degrees bend

Fig.9. Coriolis number.

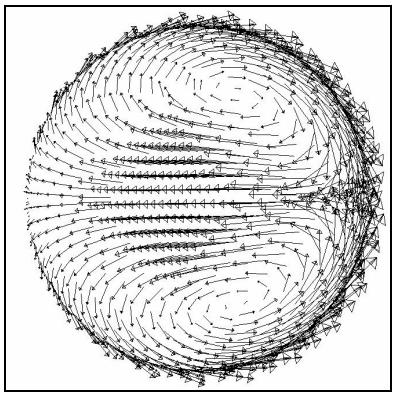

Fig.10. Velocity vectors for $\phi_1 = 90°$ (view downstream, vector scale = 1).

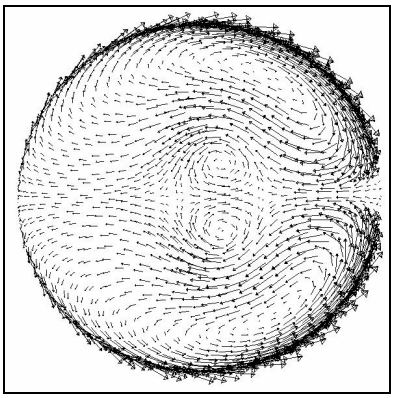

Fig.11. Velocity vectors for $\phi_2 = 60°$ (view downstream, vector scale = 1).

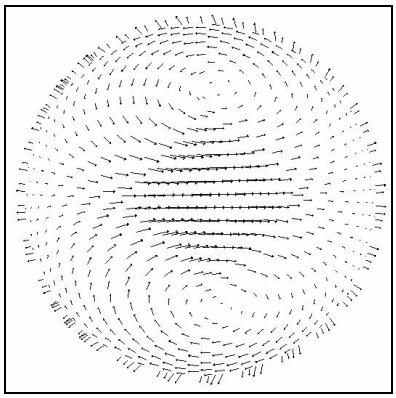

Fig.12. Velocity vectors at 12.5d behind bend (view downstream, vector scale = 14).

6.2 S-bend

Vortex pair originates after fluid passes bend inlet due to radial pressure gradient. Velocity maximum is on the concave side just behind the end of the first bend. Pressure gradient in the second elbow is about 10% higher than in the first one. This results in fluid displacement towards the inner side of the second bend, which is documented by distinct peak in Coriolis number profile. Coriolis number and naturally also kinetic energy reaches the highest value of all investigated geometrical configurations. This is reflected by highest minor loss coefficient.

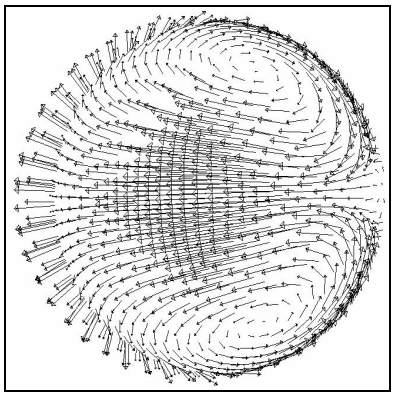

Fig.13. Velocity vectors for $\phi_1 =$ $= 90°$ (view downstream, vector scale = 1).

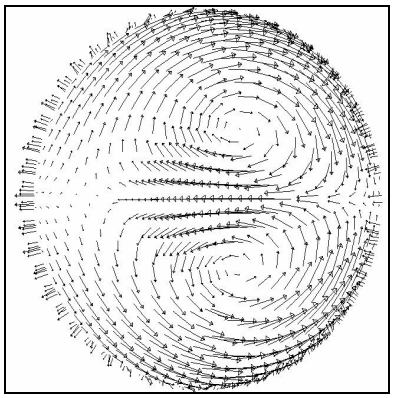

Fig.14. Velocity vectors for $\phi_2 =$ $= 90°$ (view downstream, vector scale = 1).

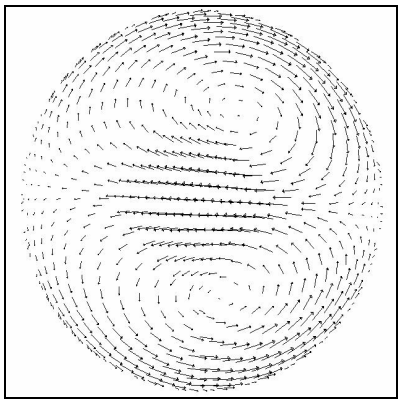

Fig.15. Velocity vectors at 25.d behind bend (view downstream, vector scale = 3).

6.3. Spatial 90-degrees bend

Pressure gradient in the second bend is rotated by 90 degrees, which induces flow field deformation, see fig.17. Axial velocity distribution together with centrifugal force invokes helical flow pattern with one vortex. Flow in spatial 90-degrees bend is associated with 3 peaks of kinetic energy profile: behind the first bend inlet, behind the first bend exit and behind the second bend exit. Minor loss coefficient is lower than for S-bend, which is in discrepancy with [5]. However result of computational simulation is well justified by kinetic energy and Coriolis number profiles.

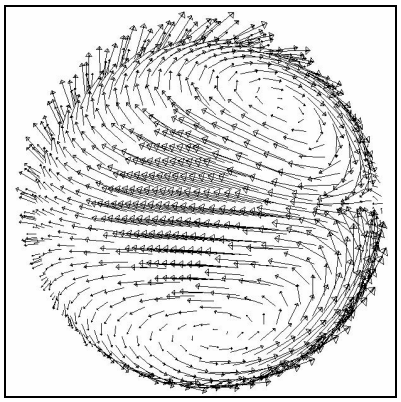

Fig.16. Velocity vectors for ϕ_1 = 90° (view downstream, vector scale = 1).

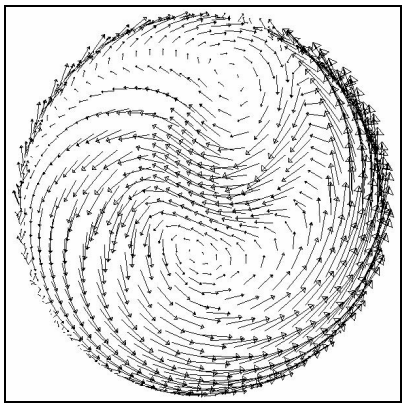

Fig.17. Velocity vectors for ϕ_2 = 40° (view downstream, vector scale = 1).

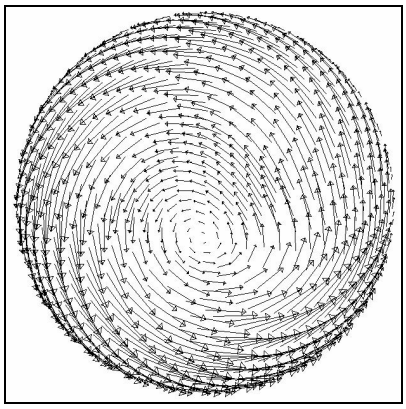

Fig.18. Velocity vectors at 12.5d behind bend (view downstream, vector scale = 2).

7. Minor loss coefficient

Minor loss coefficients were evaluated according to eq.(19) and are summarized in tab.2. Differences are apparent for all geometrical configurations. Major disagreement is for U-bend and spatial 90-degrees bend. It is important to note that the outlet evaluation cross-section was $32.5.d$ behind last bend (i.e. $2.5.d$ in front of outlet boundary condition) for all configurations. Longer outflow pipe ($60.d$) was created behind single bend to investigate how far the flow recovery region reaches. It was discovered that it is not less than $40.d$, where flow is fully recovered and minor loss coefficient attains final constant value. This in contrast with well known rule of thumb, which recommends to place pressure transducers $10.d$ behind the last bend. However it is approximately distance $10.d$, where the flow is already considerably recovered and slow recovering process continues along distance of approximately another $30.d$, see fig. 19.

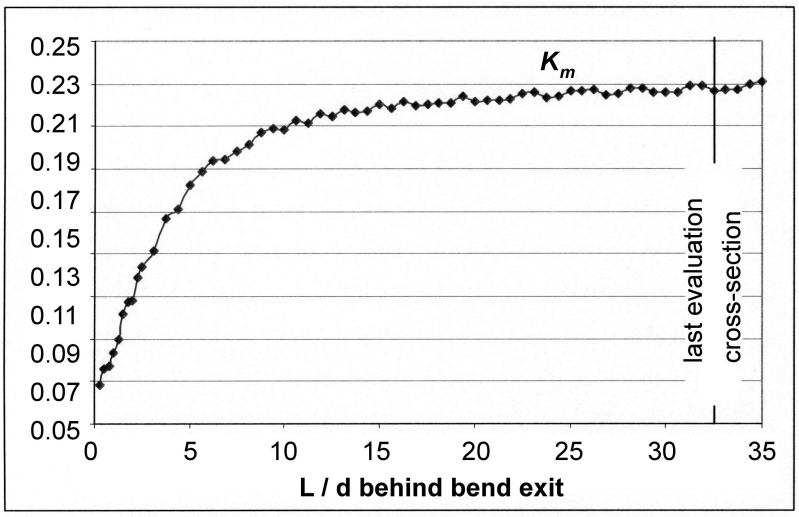

Fig.19. Minor loss coefficient profile for single bend.

	single bend (out-flow length = 35.d)	single bend (out-flow length = 60.d)	U-bend	S-bend	Spatial 90-degrees bend
Computational simulation	0.1769	0.2254	0.159	0.2932	0.277
Experiment [5]	0.219	0.219	0.300	0.3723	0.438

Tab.2. Minor loss coefficient.

8. Conclusion

A numerical simulation of turbulent flow in different geometrical configurations composed of curved bends was performed. Velocity vector fields on bend cross-sections were recorded and put in connection with Coriolis number and kinetic energy of the respective cross-section.

Presented study reveals that principal integral characteristics are reflection of the flow field details. Energy dissipation of flows in curved ducts originates from mutual transformations of kinetic and pressure energy that are invoked by centrifugal forces. This conclusion explains the least minor loss coefficient of U-bend, where the flow uniformity is enforced by two pairs of counter-rotating vortices and the biggest coefficient for S-bend, where one massive vortex pair originates and the flow is characterized by large velocity difference in radial direction.

Finally it should be concluded that the flow recovery is rather slow process reaching more than 40.*d* behind the last bend. This should be kept in mind especially when placing measurement equipment (e.g. pressure transducers, flowmeters).

Acknowledgements

The work has been supported by the grant project of Grant Agency of the Czech Republic No 101/06/P190 "Shape Optimization of the Diffuser with Inlet Circumferential Velocity Component".

References

[1] U. Andersson, T.F. Engstrom, L.H. Gustavsson, R.I. Karlsson, The Turbine 99 Workshops - Conclusions and Recommendations, Proc. 22nd IAHR Symposium, Stockholm, 2004.
[2] M. Desová, Nature of Flow and Hydraulic Losses in Tandem Elbows, Diploma thesis, 2006 (in Czech).
[3] Fluent 6.2, Fluent. Inc, Lebanon.
[4] H. Iacovides, B.E. Launder, H-Y. Li, The computation of flow development through stationary and rotating U-bends of strong curvature, International Journal of Heat and Fluid Flow, Vol. 17, 1995, pp.22-28.
[5] I.E. Idělčik, Spravočnik po gidravličeskim soprotivlenijam, Mašinostrojenije, Moskva, 1975 (in Russian)
[6] D.S. Miller, Internal Flow, BHRA, Cranfield-Bedfors, 1971.
[7] M. Raisee, H. Alemi, H. Iacovides, Prediction of developing turbulent flow in 90°-curved ducts using linear and non-linear low-Re k-ε models, International Journal for Numerical Methods in Fluids, 51(12), 2006, pp. 1379-1405.
[8] P. Rudolf, Modeling of Secondary and Separated Flow in Curved Channels of Rectangular Cross-Section, Proceedings of Topical Problems of Fluid Mechanics, 2004, Prague.
[9] P. Rudolf, Analysis of Flow in Elbow of Rectangular Cross-Section, Proceedings of "Engineering Mechanics 2003", Svratka, 2003 (in Czech).
[10] K. Sudo, M. Sumida, H. Hibara: Experimental Investigation on Turbulent Flow in Circular-Sectioned 90-Degree Bend, Experiments in Fluids 25 (1998) 42-49.
[11] K. Sudo, M. Sumida, H. Hibara: Experimental Investigation on Turbulent Flow through a Circular-Sectioned 180° Bend, Experiments in Fluids 28 (2000) 51-57.